II.2.4 Functionally Designed Ultra-Lightweight Carbon Fiber Reinforced Thermoplastic Composites Door Assembly (Clemson University)

Dr. Srikanth Pilla, Principal Investigator
Department of Automotive Engineering
Department of Materials Science and Engineering
Clemson University
4 Research Dr., Suite 340
Greenville, SC, 29607
E-mail: spilla@clemson.edu

Dr. H. Felix Wu, DOE Technology Manager
U.S. Department of Energy
E-mail: felix.wu@ee.doe.gov

Start Date: December 1, 2015 End Date: November 30, 2020
Project Funding (FY 19): $1,424,056 DOE share: $643,239 Non-DOE share: $780,817

Project Introduction

One of the most promising routes for achieving the 2025 Corporate Average Fuel Economy standards involves decreasing vehicular weight by incorporating lightweight materials, coupled with component redesign, in order to improve overall fuel efficiency. Indeed, one recent study indicates that the simple replacement of current metallic doorframes with carbon fiber-reinforced polymer composites can reduce the overall weight of the component by nearly 58% [1]. The objectives of this project are to achieve a weight reduction of at least 42.5%, as compared to the baseline door structure, at a cost of less than $5/lb. while saving on energy metrics without compromising the fit, function, crash, and noise, vibration and harshness requirements. The strategy for achieving these targets involves a holistic systems approach through the integration of unique designs, novel materials, manufacturing technologies, and joining/assembly of subsystems to ensure the developed technologies are ready for commercialization.

Objectives

The objective of this project is to reduce the weight of a door assembly by at least 42.5% compared to a baseline driver's side front door with an expected cost increase of less than $5/lb. in weight saved. A 2013 mid-sized sport utility vehicle's door from our OEM partner with an assumed production volume of 20,000 vehicles annually is the basis for design. These criteria will either meet or exceed the fit, function, crash, and NVH requirements of the baseline door.

The intent is to (1) enable a radical redesign of the baseline door via a holistic systems approach through the integration of unique designs, (2) use novel materials that render the door 100% recyclable and (3) investigate manufacturing technologies and joining/assembly of subsystems to ensure the developed technologies are ready for commercialization. The partner organizations listed in Table II.2.4.1 are providing highly leveraged knowledge expertise to ensure the success of this effort.

Table II.2.4.1. Project Participants.

Universities	Industry Partners	Computation Partners
Clemson University	OEM	Altair Engineering
	BASF, Polyone	Core-Tech Systems (Moldex 3D)
University of Delaware	Krauss-Maffei, Trexel Inc.	MSC Software (Digimat)
	Corning	LS-DYNA

Approach

The project entails the use of a systems-level approach that begins with a systematic evaluation and benchmarking of the door and its subassemblies. In collaboration with our partnering companies and commercial suppliers, researchers are evaluating a variety of CF thermoplastic material forms for structural components (i.e., novel unidirectional and fabric prepregs, co-mingled fabrics, high aspect ratio discontinuous fibers, performance thermoplastic resins, novel fiber architectures, and localized reinforcements) and alternative solutions for glazing, trim, and other subcomponents. The initial focus involves creating the structural component and a materials database for all parts of the door structural assembly (i.e. outer shell, inner panel, carrier, and anti-intrusion beam(s)).

A two-phase integrated design and manufacturing optimization approach was adopted to obtain the optimal manufacturing process parameters of the thermoplastic materials and the optimal structural design parameters of the door. The Principal Investigators also conducted a top-level trade study to determine at least two candidate designs for optimization. The design parameters include: (a) thermoforming and injection-molding parameters (e.g., pressure, temperature); (b) fiber parameters (e.g., material, length, diameter, volume fraction); (c) matrix parameters (e.g., material, volume fraction); (d) structural wall thickness; and (e) material density distribution. The research team will use four analysis tools: (1) Moldex3D, (2) Digimat, (3) LS-DYNA Implicit and (4) LS-DYNA Explicit to construct the manufacturing-to-response analysis pathway [2–4]. The team will fabricate a door based on this optimal design for testing in accordance with OEM performance requirements.

Results

Concept Development

The team's focus in the fourth year was on designing for mass reduction, meeting static and dynamic crash targets, and improvement in manufacturability. In order to achieve the mass reduction target, the team performed three major revisions, as seen in Figure II.2.4.1, in composite door structural design, for which several composite optimization, static and dynamic tests were carried out over FY 2019. The first revision, as seen in Figure II.2.4.1 (b), included the removal of the injection-molded sash reinforcement part and its replacement with an inner beltline stiffener (IBS) extended into the sash region. The second revision, as seen in Figure II.2.4.1 (c) was carried out on outer panel stiffener (OPS) in order to attain maximum stiffness along with cost-effective manufacturability. The team conceptualized two different versions of OPS, viz. OPS version 1 and OPS version 2 by performing topology optimization. Figure II.2.4.1 (a), (b), and (c) shows the older composite door concept—along with the two new door designs—for which results are discussed in the sections that follow. The third major revesion involved design changes, as seen in Figure II.2.4.1 (d) on the inner panel in order to improve its manufacturability. The most important changes were increasing the overall draft angle by 2–4° and removing complex features like the cavity for water bottle holder in order to simplify the design.

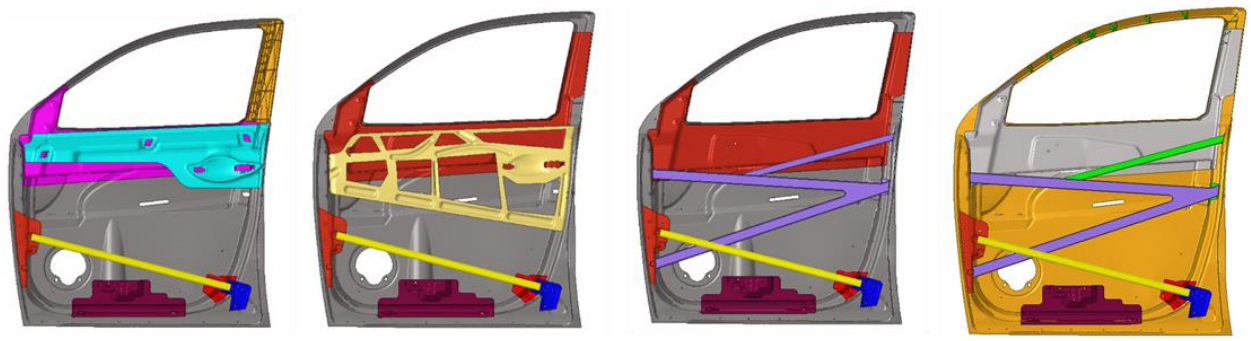

(a) (b) (c) (d)

Figure II.2.4.1. Door concept comparison: (a) composite door with older OPS design; (b) newer composite door design with OPS version 1; (c) newer composite door design with OPS version 2; and (d) final composite door design with simplified inner panel geometry and OPS version 2. Source: Clemson University.

Summary of FEA Results

The team assesed the existing unidirectional (UD) ply design, which included the extention of the IBS into the sash region and the extruded OPS design presented in Figure II.2.4.2 (a). Upon considering the thermoforming complexity of the UD ply setup, the team reassessed the design and came up with a mixed setup of woven and UD plies for inner panel. The new inner panel layup is presented in Figure II.2.4.2 (b), where the bottom-most 4-plies are woven (0/90 45/-45) and shaped like the inner panel minus the sash region, while the UD plies are laid over the woven plies in a quasi-isotropic manner. This layup would help in performing the thermoforming operation, since the four bottom woven plies are easily drapable and would require less darts and cuts, thus reducing the number of plies at the bottom. This will ensure that plies remain intact during the high-heating process. Considering this mixed-ply setup, several design iterations were performed to achieve the target weight while satisfying both linear and nonlinear load cases. Composite optimization was first undertaken for static load cases. These load cases were obtained both from the literature as well as from specific requirements provided by our OEM partner. Eleven static load cases and design constraints are prescribed on structural parts: (1) door sag (two subcases); (2) sash rigidity (two subcases); (3) door over opening; (4) beltline stiffness; (5) outer panel stiffness; (6) mirror mount rigidity (two subcases); (7) speaker mount rigidity; and (8) window regulator stiffness. Given the absence of OEM design constraint requirements for beltline stiffness, door over opening, and mirror mount stiffness, we obtained these requirements by applying the same load cases as on the baseline steel door. It is to be noted that the BIW component is eliminated in optimization runs to ensure a higher computational efficiency. Also, the effect of BIW deformation is incorporated by adjusting the door sag requirement via considering BIW deformation at the hinges.

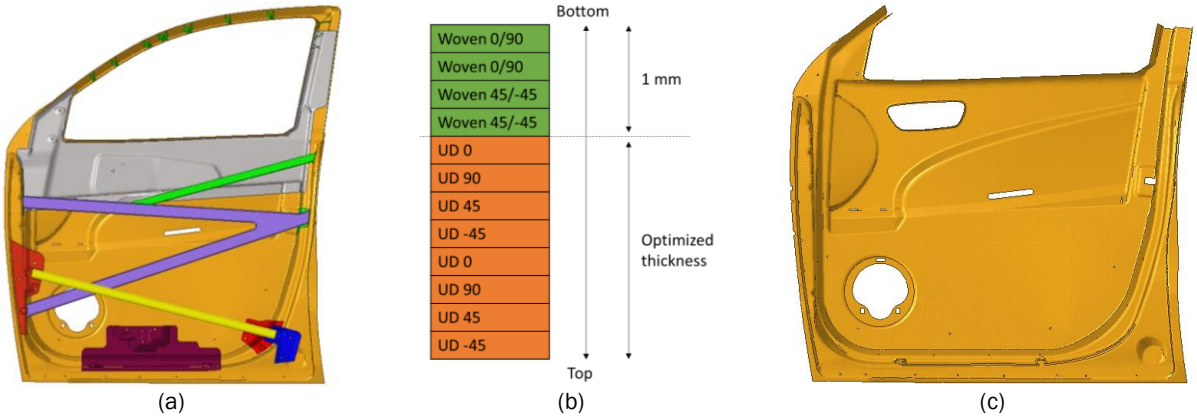

(a) (b) (c)

Figure II.2.4.2. (a) Latest door design; (b) new ply layup with mixed woven and UD plies; and (c) shape of bottom four woven plies. Source: Clemson University.

The ply layup obtained from the drape simulation is used to setup the composite optimization problem in the Altair software suite. The design obtained from the initial optimization under linear static load cases is presented in Figure II.2.4.3. The weight of inner panel is 2.6 kg, while its minimum thickness is 1.1 mm. The IBS weighs 0.475 kg with a minimum thickness of 0.5 mm. Since composite optimization is carried out only for static load cases, it still needs to be refined for dynamic load cases. In order to resolve this, a quasi-static pole (QSP) test is carried out first on the presented optimized design. Subsequently, regions that were failing early in the test were identified, thickness was manually increased, and the tests were repeated. After a few iterations, a final design was achieved for the two versions, such that it satisfied both linear and nonlinear load cases. The final design that satisfied both static and dynamic load cases is shown in Figure II.2.4.4. The weight of the IP is obtained as 3.57 kg, while that of the IBS is 0.61 kg. The minimum thickness of inner panel is 1.1 mm, while its maximum thickness is 3.4 mm in some parts of the sash region. The minimum thickness of the IBS is obtained as 0.5 mm, while its maximum thickness is found to be 4.8 mm in the mirror mount region. In order to satisfy the sash A and B load cases and constrain the maximum thickness (for ease of manufacturability), 1.2-mm steel ribs were placed in the sash region at ten locations that weigh ~ 0.2 kg. The static results with the final design are presented in Table II.2.4.2. It can be seen that all of the static load cases are satisfied with this design (values in bold green), and when compared with the baseline structure, the composite door structure weighs 56% less; however, the total weight of the door is lowered by 35%, which is 7% higher than DOE's target.

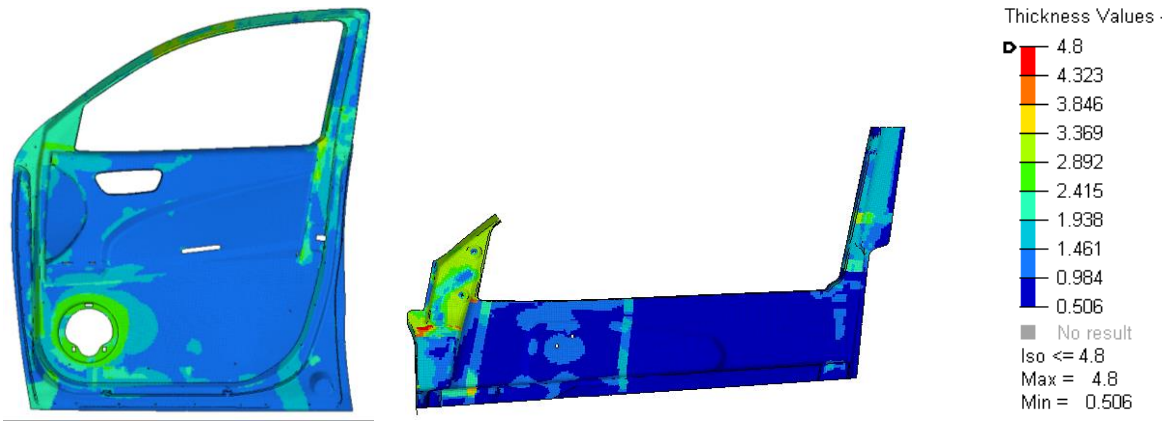

(a) (b)

Figure II.2.4.3. Thickness distribution obtained after static optimization under linear load cases for the door components: (a) inner panel and (b) IBS. Source: Clemson University.

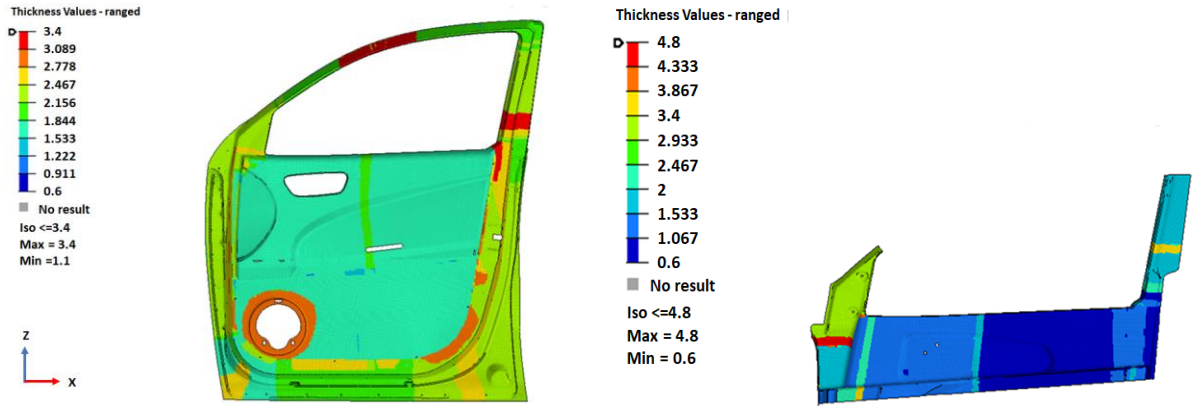

(a) (b)

Figure II.2.4.4. Thickness distribution of the door components: (a) inner panel; and (b) IBS, which satisfies both linear and nonlinear load cases. Source: Clemson University.

Table II.2.4.2. Static Performance of Composite Door.

Serial No.	Target Category Subcase	Target (Unit)	Target (Unit)	% Relative Difference (Result-Target/Target)
1	Mass Target			
1.1	–	Structural Frame Mass	< Baseline (Kg)	-56%
1.2	–	Total Weight	< Baseline (Kg)	-35%
2	Frame Related			
2.1	–	Door Sag – Fully Open	< Baseline (mm)	-68%
2.2	–	Sash Rigidity at Point A		-4%
2.3	–	Sash Rigidity at Point B		-35%
2.4	–	Beltline Stiffness – IP		-63%
2.5	–	Window Regulator (Normal)		-6%
2.6	–	Mirror Mount Rigidity in X		-4%
2.7	–	Mirror Mount Rigidity in Y		-68%
2.8	–	Door Over Opening		-6%
2.9	–	Speaker Mount Stiffness		-3%

Nonlinear Load Cases

The composite door designs discussed in the previous section were further tested for nonlinear load cases to evaluate their crashworthiness. These load cases are (a) the QSP; (b) the full pole test (using the Japanese New Car Assessment Program AF05 female dummy) and (c) the deformable barrier test (Insurance Institute for Highway Safety Side-Impact Moving Deformable Barrier (IIHS SI MDB)) and the requirements of were provided by our OEM partner. The QSP test is evaluated by plotting the reaction force against pole displacement for each design. The area under the curve of this plot gives the energy absorbed during pole impact. Figure II.2.4.5 presents a plot comparing the baseline steel door and the composites door, which display the plot for the first stage (stroke < 6 in.) and the second stage (stroke < 12 in.). The initial average crush for the composite door is 22% higher than the actual OEM requirement. The intermediate crush (until 12 in.) is seen to be 85% higher than the actual OEM requirement. Figure II.2.4.5 presents the reaction force plot until the 18 in. of stroke for baseline and composite doors. It can be clearly seen from the plot that composite door satisfies the maximum peak crush requirement (horizontal dashed line in the plot) and is higher by 133%. These results for the QSP load case are listed in Table II.2.4.3.

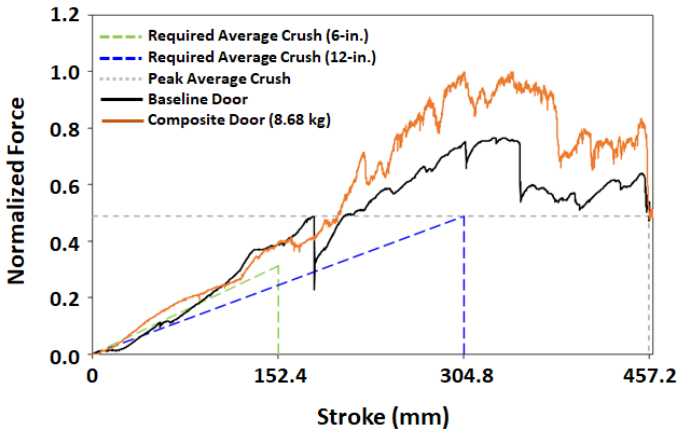

Figure II.2.4.5. Reaction force plot for the QSP test comparing the baseline door with the composite door.
Source: Clemson University.

Table II.2.4.3. Results for the QSP Test.

Results	% above OEM requirement
Initial Average Crush	122%
Intermediate Average Crush	185%
Peak Crush	233%
Initial Average Crush	122%

The dynamic simulations for the deformable barrier and the full pole load cases were then performed for both versions. To evaluate the performance of the doors, the team—after discussion with OEM partner—listed key performance indicators. Further, a gauging matrix was created to assess whether the composites door passed the OEM requirements. The gauging matrix was defined as: (a) successful (green), if the door response is better than the baseline; (b) tolerable (yellow), if the door response is lower than the baseline, but within a 10% margin; and (c) failure (red), if the door response is below 10% from the baseline door. Table II.2.4.4 shows the results for the deformable barrier load case test, comparing the composite door with the baseline responses. The composite door response for the full pole (using the AF05 female dummy) is also presented and compared with the baseline door in Table II.2.4.4. The composite door responses either exceed or are within the tolerable range for both load cases.

Table II.2.4.4. Results For Full Pole and Deformable Barrier Dynamic Load Cases.

Key Performance Indicator	Target	FMVSS 214 Rigid Pole (Response/Target) %	IIHS SI MDB (Response/Target) %
Max center pillar intrusion	Baseline	-1%	N/A
Max sill intrusion		-11%	N/A
Max roof intrusion		-10.4%	10.8%
Max window-sill intrusion		-4.78%	11.25%
Front door dummy hip intrusion		-9.71%	18.3%
Max door lower intrusion		7%	1%
Safety survival space		N/A	2.46%
Gauging Metrics Green (Success) – Below Baseline target values (<b). Yellow (Tolerable) – More than Baseline values but smaller than 10% difference (>b, <b+10%). Red (Failure) - More than 10% above Baseline value (>b+10%).			

Subcomponent Manufacturing, Modeling, and Testing

To verify crash simulations, a subcomponent test with validation was proposed and untertaken. A hat-stiffened panel was manufactured and tested to assess simulation predictions and compare with the experimental results. The tool that was used in the subcomponent fabrication is shown schematically in Figure II.2.4.6. The material selected was AS4 CF with nylon (PA6) having a quasi-isotropic orientation for both the hat and the flat section. This material was received in the form of a prepreg tape from Tencate and was used to fabricate the subcomponent. Both parts (hat and flat section) were manufactured separately with process conditions similar to those used to generate material property data, followed by bonding with the Plexus MA530 adhesive. The Plexus system has been characterized, while the adhesive material model is being implemented in crash simulations.

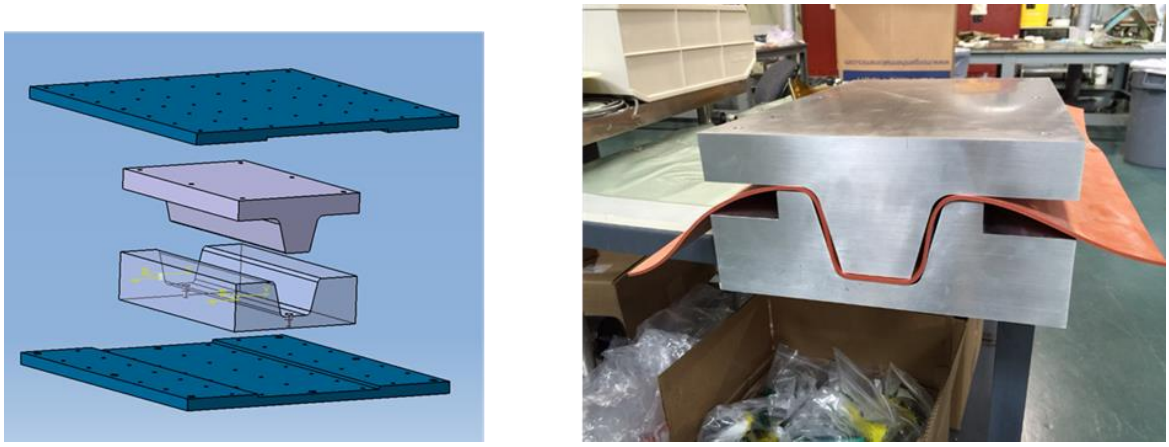

Figure II.2.4.6. Subcomponent tool for hat production. Source: University of Delaware.

The selected subcomponent geometry was comprised of two composite parts: (1) the hat and (2) the spine. The hat is a 16-layer laminate that was fabricated from $[45/-45]_s$ construction, with the spine fabricated from a quasi-isotropic construction. In both cases, flat panels were initially fabricated to appropriate geometries. The unidirectional AS4/nylon prepreg was cut and laid up to create the desired geometry and layup sequence in a flat laminate form. After layup, the prepreg stacks were autoclaved with the cycle shown in Figure II.2.4.7.

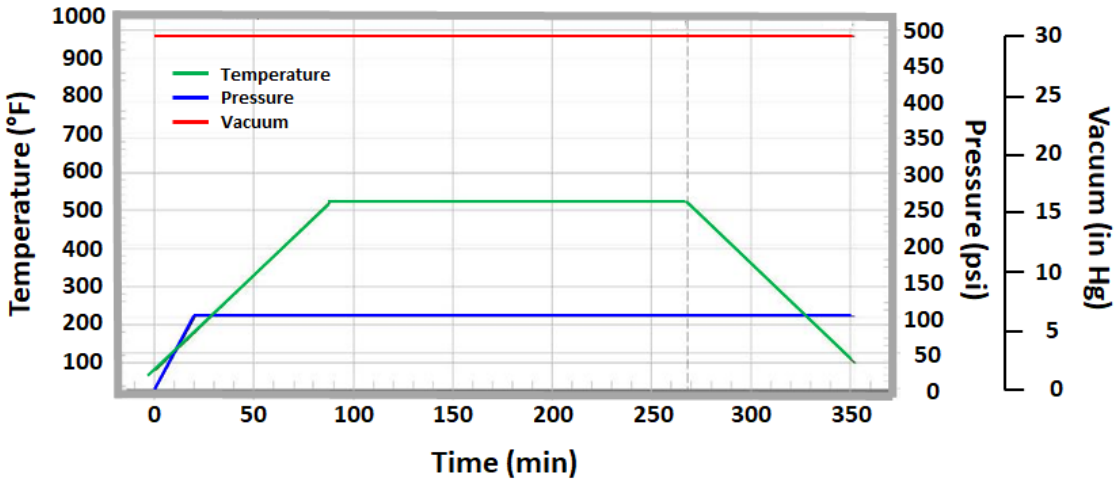

Figure II.2.4.7. Process conditions used to fabricate subcomponent. Source: University of Delaware.

A pressure of 100 psi was used to consolidate the prepreg sheets at a temperature of 520 °F and 28 in Hg vacuum for 190 min, based on the Tencate recommended process cycle shown in Figure II.2.4.8. Flat laminates were examined visually and with ultrasonic scans for quality assessment. The spine seen in Figure II.2.4.8 (a) is a flat laminate to close the hat geometry and no further processing was needed. The hat geometry seen in Figure II.2.4.8 (b) was formed from the flat laminate via the combination of temperature and pressure on an Al tool. The flat laminate was first vacuum-formed to shape in an oven at 450 °F to achieve the same shape of the tool, followed by autoclave cycle to re-consolidate the geometry to maintain laminate quality. An Al shim was used on the top surface for good surface finish and consistent thickness. The finished spine and the hat sections are shown in Figure II.2.4.8 (c).

(a) (b) (c)

Figure II.2.4.8. (a) Fabricated spine; (b) hat geometry tool; and (c) finished hat section. Source: University of Delaware.

After fabrication of the hat and spine sections, thickness measurements were taken for each section at more than 22 locations. These locations are marked hat section in Figure II.2.4.9 (a) and for the spine section in Figure II.2.4.9 (b). The hat has an average thickness of 2.32 mm with a standard deviation of 0.54 mm, while the spine has an average thickness of 2.26 mm with a standard deviation of 0.069 mm. As mentioned above, these average thicknesses were used to determine the average ply thickness in the simulation.

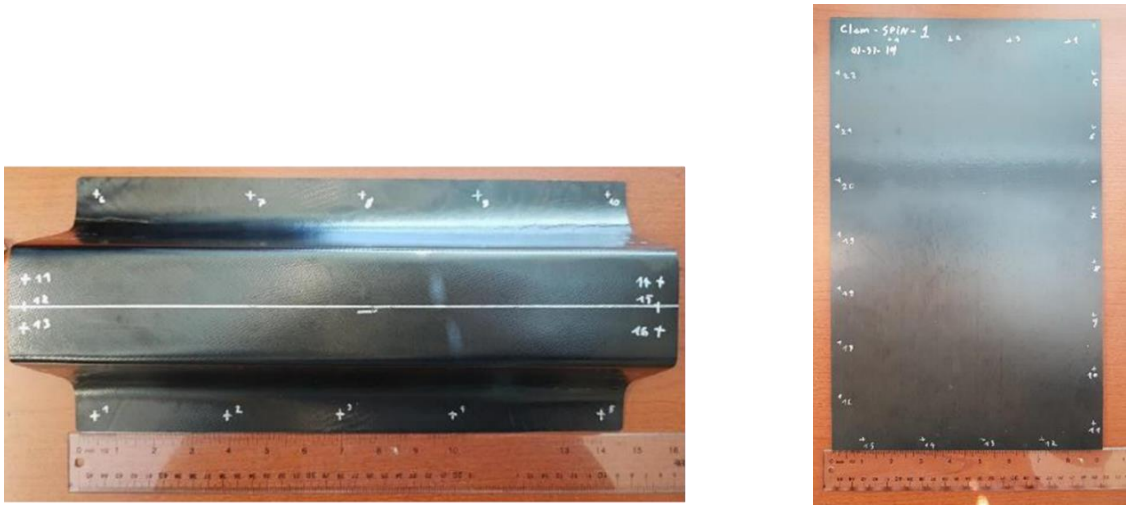

(a) (b)

Figure II.2.4.9. Measurement points of: (a) hat; and (b) spine for thickness. Source: University of Delaware.

The assembly of the hat and spine was performed with adhesive-bonding. Plexus MA530 adhesive was chosen for this purpose based on prior testing of the adhesive and its performance assessment in coupon tests. Bond line thickness was chosen as 1 mm to provide a sufficient gap tolerance for full-scale door assembly. An adhesive cure schedule was developed by Clemson University during the adhesive performance assessment, and the same cure schedule was adopted here. The final bonded assembly was put together with 1-mm spacers at three locations along the length of the bond line. Surface preparation of the bond line interfaces were comprised of grit blasting with fine SiC of 120 grit size using a thin pencil blaster for good dimensional control and was followed by wiping with a cheesecloth. Paste adhesive was applied using a standard two-component adhesive applicator and was held in place with weights to provide sufficient pressure to ensure a 1-mm bond line thickness. The completed subcomponent assembly can be seen in Figure II.2.4.10.

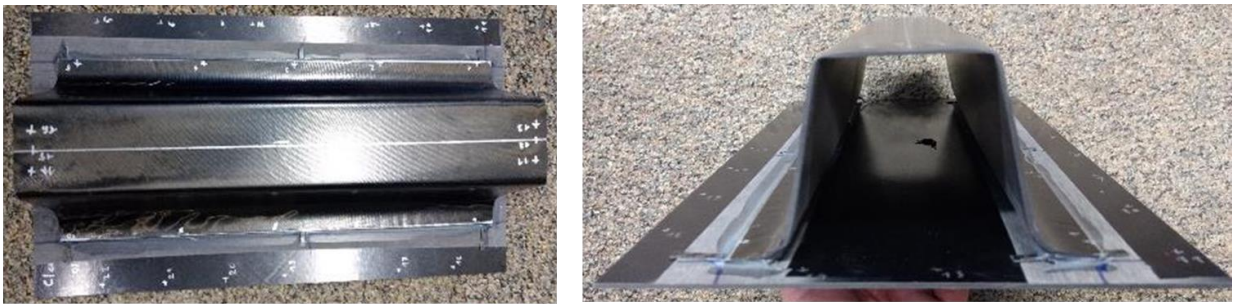

(a) (b)

Figure II.2.4.10. Completed subcomponent assembly after adhesive-bonding: (a) top view; and (b) end view.
Source: University of Delaware.

The subcomponent model consists of five-part definitions: (1) the support, (2) the impactor, (3) the hat (top half of the closed hat section), (4) the spine (base of the closed hat section) and (5) the adhesive used to bond the hat and the spine. The supports, as well as the punch, are modeled as rigid cylinders. The diameters for both support cylinders are one inch, while the punch is 2-in. The supports are constrained in all six degrees of freedom and the punch is only allowed to move in a global *z*-direction. The weight of the punch had been set to 80 kg, which had an initial velocity of 2.8 m/s that is equal to a fall distance of 15 in. and an impact energy of 300 J. The hat and the spine are modeled as PART_COMPOSITE card with 16 layers. The layup sequence for the hat is $[45/\text{-}45]_s$ and for the spine is $[0/90/45/\text{-}45]_s$. To match the thickness of the hat and the spine, measurements were taken, and an average ply thickness was calculated for the actual parts fabricated. The adhesive was modeled with an element formulation 20 and material card MAT_138, which is a mixed-mode traction and separation law. The attachment between the composite parts and the adhesive had been modeled with a CONTACT_TIED_SHELL_EDGE_TO_SURFACE contact. The bond lines are 1-mm-thick × 1-in. wide with this geometry maintained in the fabricated subcomponent. A summary of this setup is shown in Figure II.2.4.11.

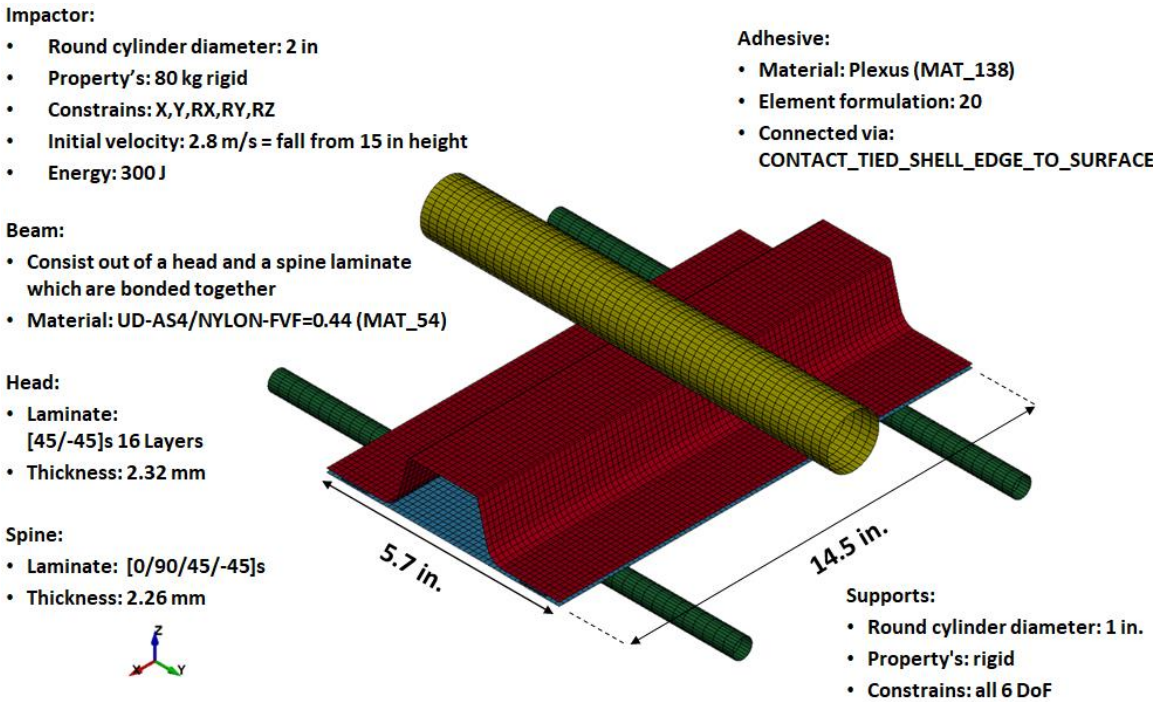

Figure II.2.4.11. Subcomponent configuration, boundary conditions, and simulation summary.
Source: University of Delaware.

The contact between the subcomponent and the supports, as well as the impactor, is modeled as the AUTOMATIC_SINGLE_SURFACE where the adhesive is excluded. In order to avoid the undesirable oscillation in contact, viscous damping is implemented at 20%, which is the LS-DYNA recommended value for metallic and similar material contacts. This value is also used to define surface contacts in nonlinear load cases. Bulk viscosity and hourglass viscosity are set to a default value. The static and dynamic coefficients of friction between all parts that are included in the single surface contact is set to 0.08. To speed up the simulation runtime, mass scaling was used, while the artificial mass increase was < 0.33% of the original mass, which accounts for a time step of 5.500e-07s.

Simulation results showed that the hat section of the beam will locally fail, but the structure itself will withstand the impact. No bond line failure was observed in the course of simulation. The maximal contact force between the impactor and the beam is predicted to be around 10 kN at around 0.004 s. The predicted force–time plot is shown in Figure II.2.4.12.

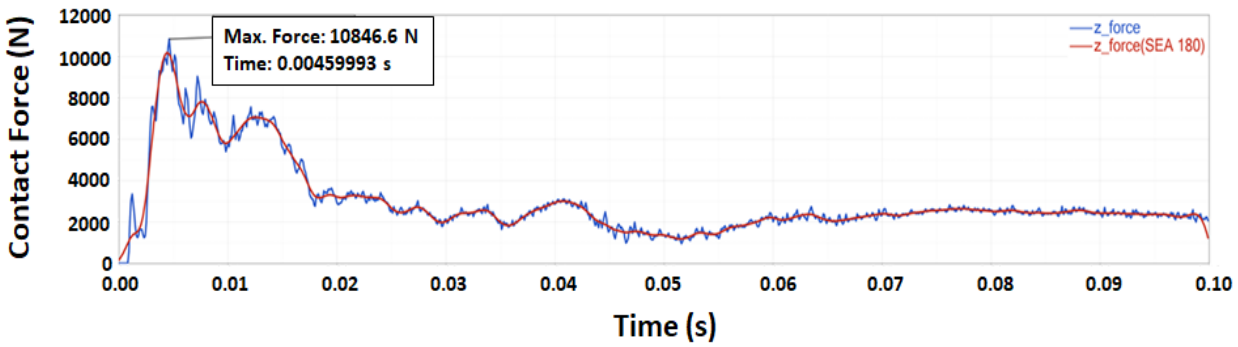

Figure II.2.4.12. Predicted contact force over time for the simulation conditions in Figure II.2.4.13.
Source: University of Delaware.

Impact testing was performed at the University of Delaware, Center for Composite Materials, using their 1100 J drop tower and a 2-in. cylindrical impactor with 1-in. round cylindrical supports, as modeled. The subcomponent is simply supported on its supports, prior to an impact drop. The impact energy of 300J is selected by observing failure from initial numerical simulations. The impactor has a fixed weight of 80 kg while drop height is adjusted to 15 in. such that total impact energy matches 300J, which is the energy level where the initial simulations showed failure. The following were part of the test setup:

1. Strain gauges at key locations on the hat and the spine.
2. Load cell in the impactor for force response.
3. Spine center deflection is been measured with a laser displacement center.
4. High-speed video to capture dynamic deformation of the spine (side view).

Multiple biaxial strain gauges (two at the bottom and one on the side) were adhesively bonded onto the fully assembled subcomponent at locations that are predicted to experience higher strain determined from the simulations, as shown in Figure II.2.4.13.

(a) (b)

Figure II.2.4.13. Location of the bonded strain gauges on (a) the side and (b) bottom in order to record strain during impact. Source: University of Delaware.

The 1100 J drop tower with the 80 kg impactor and strain gauges were calibrated, and the test was carried out in accordance with the simulated test conditions. Excerpts from the high-speed camera are shown in Figure II.2.4.14, which show the impactor and subcomponent before the impact, at the moment of the impact, and after the impact.

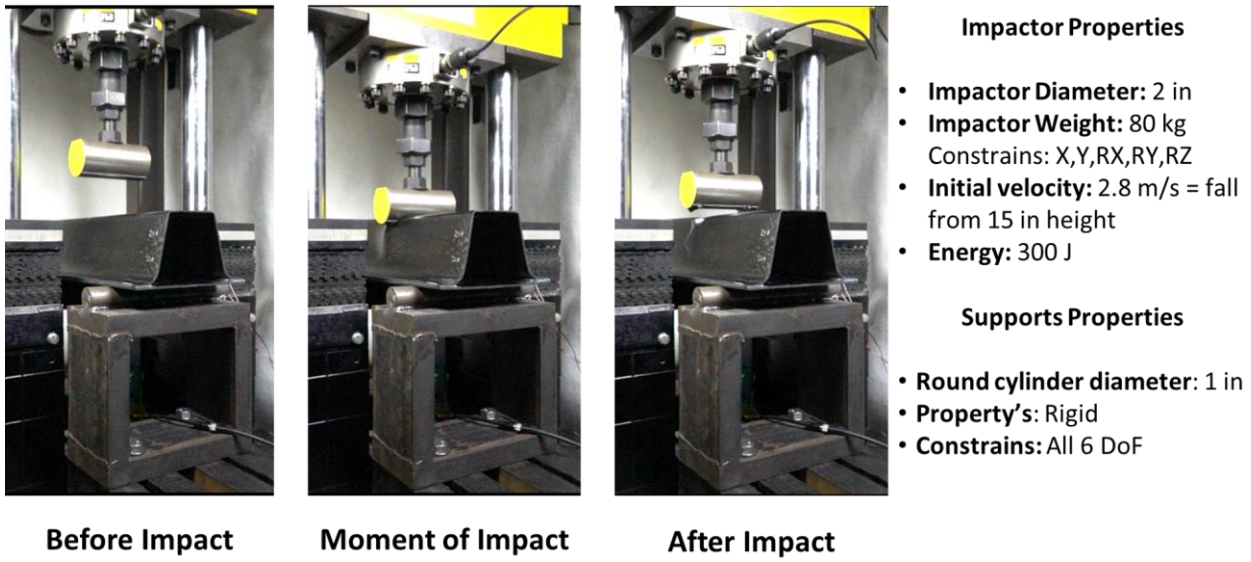

Figure II.2.4.14. Subcomponent test progression showing the impactor and the subcomponent before the impact, at impact, and after the impact. Source: University of Delaware.

A preliminary comparison between the simulated and experimental results of the test revealed that the simulated contact force was lower than expected, as observed in Figure II.2.4.15 (a). One explanation for this could be that the model currently uses a material card where elements are deleted beyond a certain force and strain in the elastic regime. However, in reality, due to the ductile nature of the thermoplastic PA66 nylon matrix, we observe that the composite as a whole is able to absorb and withstand far higher loads without failing catastrophically if loaded in compression as can be seen by the pictures in Figure II.2.4.15 (b). The team is currently looking into the material model and will modify it and the simulation strategy to better reflect the experimental results.

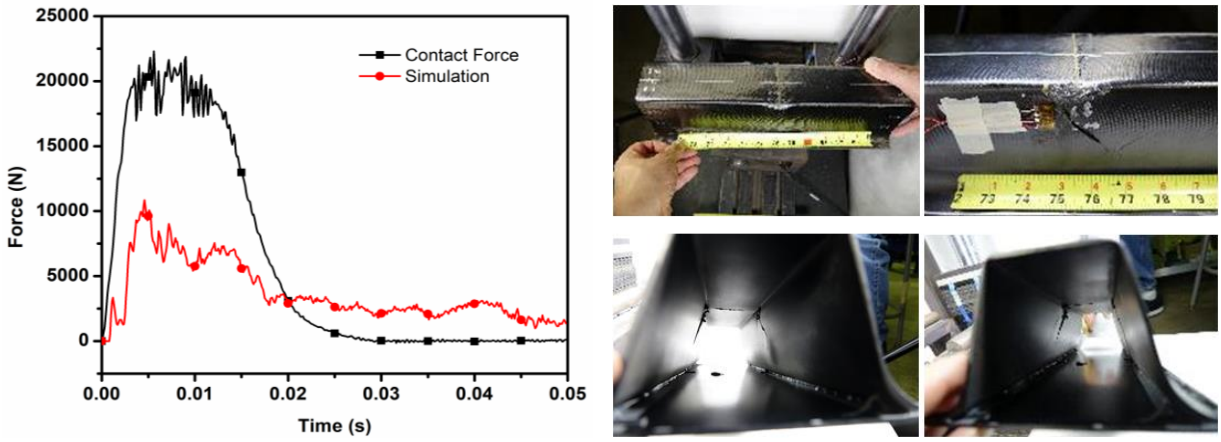

(a) (b)

Figure II.2.4.15. (a) Comparison between the simulated and experimental results. (b) If loaded, the composite, as a whole, is able to absorb and withstand far higher loads. Source: University of Delaware.

Fully Assembled Prototype Door Meeting Fit and Integration Requirements

To validate the geometry of the ultralightweight composite door, the team decided to build a 1:1 door mockup to validate the fit and function of the current composite door. In addition, an important goal set by our OEM partner was to ensure that our design maintains the same sea-lining geometry as the baseline, while housing all of the baseline equipment. The inner panel is the most crucial component of the ultralightweight composite door, primarily because all of the interface points for vehicle structure are through the inner panel. A carbon fiber-reinforced epoxy door was built primarily using the vacuum infusion process for low-cost prototyping. To keep the fabrication cost down, a wooden cavity tool was procured and finished in-house. For all other internal parts, the team decided to 3D-print them using acrylonitrile butadiene styrene material.

The wooden tool was finished using dry sandpaper from 80 grit to 400 grit in increments. Once the tool was cleaned, two coats of a polyurethane tool coat were applied to a thickness of ~ 0.5 mm and were allowed to cure for 48 h. After this, the team sanded and polished the tool further to 800 grit in order to obtain a highly smooth surface. Four coats of chemical release agent were applied to the polished tool surface. Once the tooling coat was dry, the team placed dry CF fabrics similar to the ply design, in the actual door. The lines for the vacuum and the resin flow were then laid out to optimally fill the mold, which was bagged with breather cloth and resin flow media. Once the bag was properly sealed, the vacuum of – 28 in. Hg was applied and the resin was infused. The parts were allowed to cure for 48 h in the tool, and then demolded and further cured for an additional 12 h in the oven at 65°C. The fully cured inner panel was then trimmed and painted.

The internal parts of the 3D-printed door were attached to the inner panel in addition to weather sealing. The assembled door was then installed onto the vehicle for fit and function validation. Below is the list of criteria used to verify that the designed door geometry and the 1:1 mockup fits and functions were as desired on the existing vehicle. Figure II.2.4.16 shows the manufacturing process for the 1:1 mockup with internal parts assembled on the existing vehicle.

Figure II.2.4.16. Composite door manufacturing process. Source: Clemson University.

Door fit criteria:

- The team confirmed that the current design properly fits in the existing vehicle and properly aligns with all mounting points shown in Figure II.2.4.17.
- The weather sealing is properly compressed when the door is closed to achieve good sealing.
- The door frame has enough internal space for all of the components.
- The door properly aligns with the B-pillar and the dashboard.
- The door window frame is flush with the existing interior trim.

Door function criteria:

- The door frame properly opens and closes without any interference with the existing vehicle structure and rear door.
- The door securely latches with the existing latch loupe plate.
- The door has sufficient access for assembly, disassembly, and repair of the door internal components.

During this process, the team also identified minor design improvements for ease of assembly and repair. These changes are currently being incorporated into the final computer-aided design models.

Figure II.2.4.17. Fully assembled door frame on the existing vehicle. Source: Clemson University.

Cost Modeling Summary

A generative cost model was developed to estimate the total cost of the latest design of the door, which was $989.79. Cost of the inner panel is $379, which accounts for 38% of the total cost of the door, as seen in Figure II.2.4.18. Material, tooling, equipment, labor, energy, building, maintenance, overhead, and capital were considered to calculate the cost of each individual part.

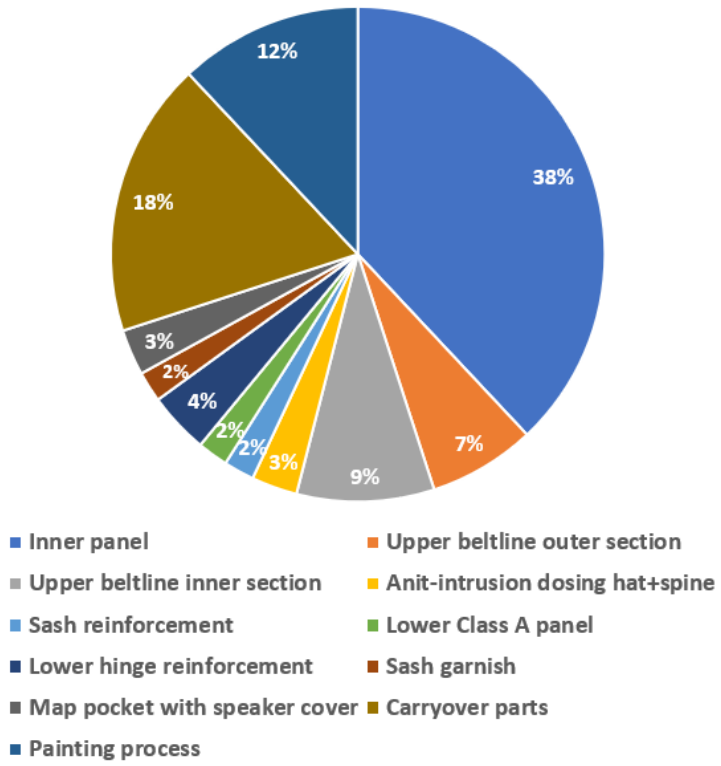

Figure II.2.4.18. Cost distribution of the individual parts of the door. Source: Clemson University.

After the development of a generative cost model, a parametric cost model was developed to find how individual parameters influenced the total cost. Parametric cost modeling was carried out in three steps: (1) development of cost estimating relationships; (2) parameterization of the door design; and (3) creation of the user interface to perform tradeoffs and estimate the cost of individual parts. The following assumptions were made for the development of parametric cost model:

1. Total cost is assumed to be a function of material, labor, equipment, tool, energy and overhead cost.
2. Parameters identified for cost estimation are independent of each other.
3. Data is collected and normalized using experience and a literature review.
4. Rate of overhead (18~24% of total cost) is assumed by experience.
5. Production volume per year is assumed to be around 20,000 vehicles.
6. Cost of carry over parts (~$183) is assumed to be constant.
7. Number of workers working on each machine are assumed to be four.

At first, individual parameters that influenced the overall cost of the door were identified, which are: (1) electricity cost per kWh, (2) scrap rate, (3) mold life, (4) equipment life, (5) labor wage, (6) production volume per year for 20,000 vehicles, (7) overhead rate and (8) material cost. Then, a relationship between these parameters with the total cost was determined using mathematical and statistical tools. The distribution plot for each of the identified parameters and the corresponding total cost was calculated and is presented in Table II.2.4.5.

Table II.2.4.5 Statistical Distribution of Individual Parameters and Total Cost.

Serial No.	Parameter	Raw data distribution	Mean ± 2 Std. Dev.	Total cost distribution	Total cost (U.S.Dollars)	Probability
1	Electricity rate (cents/kWh)	Log logistic	7.5~15	Log normal	988~991	0.94
2	Scrap rate (%)	Log normal	4~13	Largest extreme value	974~1022	0.95
3	Mold life (years)	Log logistic	3.5~12.5	Logistic	925~1136	0.96
4	Equipment life (years)	Log normal	5~13	Normal	987~992	0.94
5	Labor wage ($/hr)	Weibull	15~25	Weibull	981~1002	0.95
6	Production per year	Weibull	14500~26500	Log normal	952~1048	0.96
7	Overhead rate (%)	Normal	15~27	Normal	956~1036	0.95
8	Material cost ($)	Weibull	69~94	Log logistic	978~1054	0.95

Furthermore, the total cost is determined by incorporating all the identified parameters. Assuming normal distribution, the total cost of the door has been determined to vary between $920 and $1059, as presented in Figure II.2.4.19.

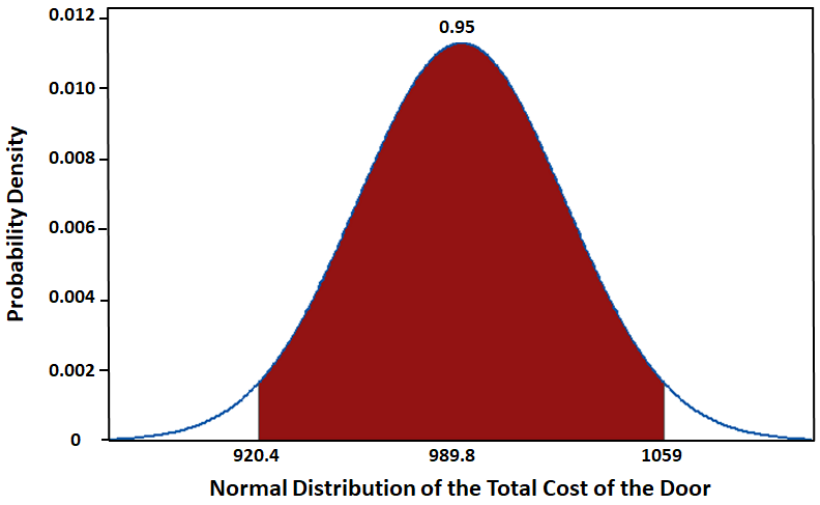

Figure II.2.4.19. Normal distribution of the total cost of the door. Source: Clemson University.

After developing the mathematical equations to determine the distribution of the total cost with a variation in identified parameters, our next step was to link the design geometry with the overall cost (i.e., parameterization of the door design). With a slight change in the geometry of the door, there will be a change in its weight, amount of raw material, and other resources used in its manufacturing, thus changing the overall cost of the door. In the last stage of efforts in FY 2019, we generated a user interface with a series of pop-up windows and dropdown menus that ask users for values of few parameters (or else, take default defined values). We could use this interface to perform tradeoffs (e.g., What-If analyses) to predict the total cost for a mix of possibilities.

Conclusions

The research focus during FY 2019 involved the modification of door design by employing an iterative processing that involved feedback from static and crash simulations, cost analysis and manufacturing constraints, while trying to comply with the aggressive weight targets. The final door design met and exceeded expectations from the viewpoint of static and crash targets. This was further validated by experimental tests performed on a subcomponent. In addition, a fully functional low-cost prototype of the design was also manufactured in order to validate fit and function requirements. From a cost perspective, the door was slightly above the cost targets primarily due to high input material costs, and strategies are being evaluated in order to meet this requirement.

Key Publications

1. Limaye, M., A. Kothari, G. Dalal, S. Pilla, and G. Li, 2019, "Manufacturing process effects on crashworthiness analysis through a numerical simulation pathway," *Society of Plastics Engineers ACCE Conference*, 4–6 September 2019, Novi, MI, USA (awarded third place in graduate student poster competition).
2. Kothari, A., M. Limaye, G. Dalal, G. Li, and S. Pilla, 2019, "Design optimization for static and crash performance of an ultra-lightweight CF reinforced thermoplastic composite vehicle door assembly," *Society of Plastics Engineers ACCE Conference*, 4–6 September 2019, Novi, MI, USA.
3. Pradeep, S. A., T. Zheng, A. Yerra, and S. Pilla, 2019, "Lightweighting class A parts via supercritical fluid assisted (ScF) injection-molding of thermoplastic olefins (TPO)," *Society of Plastics Engineers ACCE Conference*, 4–6 September 2019, Novi, MI, USA (awarded second place in graduate student poster competition).

References

1. Kelly, J. C., J. L. Sullivan, A. Burnham, and A. Elgowainy, 2015, "Impacts of vehicle weight reduction via material substitution on life cycle greenhouse gas emissions," *Environ. Sci. Technol.*, Vol. 49, No. 20, pp. 12535–12542.
2. Mi, H.-Y., X. Jing, J. Peng, L.-S. Turng, and X.-F. Peng, 2013, "Influence and prediction of processing parameters on the properties of microcellular injection-molded thermoplastic polyurethane based on an orthogonal array test," *J. Cell. Plast.*, Vol. 49, No. 5, pp. 439–458.
3. Chang, S. H. and S. S. Cheon, 2006, "In-plane directional mechanical properties of carbon fabric skins in sandwich structures after thermoforming," *Compos. Struct.*, Vol. 75, Nos. 1–4, pp. 577–581.
4. Yu, Y., J. Ye, Y. Wang, B. Zhang, and G. Qi, 2013, "A mesoscale ultrasonic attenuation FE model of composites with random-distributed voids," *Compos. Sci. Technol.*, Vol. 89, pp. 44–51.